Connective Tissue Growth Factor Is Required for Skeletal Development and Postnatal Skeletal Homeostasis in Male Mice

Ernesto Canalis, Stefano Zanotti, Wesley G. Beamer, Aris N. Economides, and Anna Smerdel-Ramoya

Department of Research (E.C., S.Z., A.S.-R.), Saint Francis Hospital and Medical Center, Hartford, Connecticut 06105; The University of Connecticut School of Medicine (E.C.), Farmington, Connecticut 06030; The Jackson Laboratory (W.G.B.), Bar Harbor, Maine 04609; and Genome Engineering Technologies (A.N.E.), Regeneron Pharmaceuticals, Tarrytown, New York 10591

Connective tissue growth factor (CTGF), a member of the cysteine-rich 61 (Cyr 61), CTGF, nephroblastoma overexpressed (NOV) (CCN) family of proteins, is synthesized by osteoblasts, and its overexpression inhibits osteoblastogenesis and causes osteopenia. The global inactivation of *Ctgf* leads to defective endochondral bone formation and perinatal lethality; therefore, the consequences of *Ctgf* inactivation on the postnatal skeleton are not known. To study the function of CTGF, we generated $Ctgf^{+/LacZ}$ heterozygous null mice and tissue-specific null *Ctgf* mice by mating *Ctgf* conditional mice, where *Ctgf* is flanked by lox sequences with mice expressing the Cre recombinase under the control of the paired-related homeobox gene 1 (*Prx1*) enhancer (*Prx1-Cre*) or the osteocalcin promoter (*Oc-Cre*). $Ctgf^{+/LacZ}$ heterozygous mice exhibited transient osteopenia at 1 month of age secondary to decreased trabecular number. A similar osteopenic phenotype was observed in 1-month-old *Ctgf* conditional null male mice generated with *Prx1-Cre*, suggesting that the decreased trabecular number was secondary to impaired endochondral bone formation. In contrast, when the conditional deletion of *Ctgf* was achieved by *Oc-Cre*, an osteopenic phenotype was observed only in 6-month-old male mice. Osteoblast and osteoclast number, bone formation, and eroded surface were not affected in *Ctgf* heterozygous or conditional null mice. In conclusion, CTGF is necessary for normal skeletal development but to a lesser extent for postnatal skeletal homeostasis. **(*Endocrinology* 151: 3490–3501, 2010)**

Cysteine-rich 61 (Cyr 61), connective tissue growth factor (CTGF), nephroblastoma overexpressed (NOV) (CCN) and Wnt-inducible secreted proteins (WISP) 1, 2, and 3 are a family of cysteine-rich secreted proteins (1, 2). CCN proteins are structurally related and share four distinct modules: 1) an IGF-binding domain, 2) a von Willebrand type C domain, 3) a thrombospondin-1 domain, and 4) a C-terminal domain, the latter absent in WISP-2 and important for protein interactions (1, 2). CCN proteins bear a structural relationship with certain bone morphogenetic protein (BMP) antagonists, such as twisted gastrulation and chordin, and can have important interactions with regulators of osteoblast cell growth and differentiation (3).

CTGF is expressed in bone and cartilage; and in osteoblasts, CTGF expression is induced by BMP, TGF-β, and Wnt (4, 5). In addition, CTGF has important interactions with these signaling molecules. CTGF binds to BMP and Wnt coreceptors and can decrease BMP and Wnt signaling (6, 7). CTGF enhances TGF-β activity and mediates effects of TGF-β on mesenchymal cell condensation (6, 8). In addition to its interactions with members of the TGF-β

ISSN Print 0013-7227 ISSN Online 1945-7170
Printed in U.S.A.

doi: 10.1210/en.2010-0145 Received February 12, 2010. Accepted May 4, 2010.
First Published Online June 9, 2010

Abbreviations: BAC, Bacterial artificial chromosome; BMD, bone mineral density; BMP, bone morphogenetic protein; CCN, Cyr61, CTGF, NOV; CMV, cytomegalovirus; COIN, conditional by inversion; μCT, microcomputed tomography; CTGF, connective tissue growth factor; CTX, C-terminal cross-linked telopeptide of type I collagen; Cyr 61, cysteine-rich 61; E10.5, d 10.5 of embryonic life; ES, embryonic stem; FBS, fetal bovine serum; FLP, flippase; GFP, green fluorescent protein; NOV, nephroblastoma overexpressed; RPL38, ribosomal protein L38; WISP, Wnt-inducible secreted protein.

superfamily and Wnt, CTGF inhibits Notch signaling in osteoblastic cells, and Notch receptors play a critical role in cell fate decisions (9–11).

CTGF regulates different cellular events, including adhesion, proliferation, migration, and differentiation. Targeted disruption of *Ctgf* in mice leads to perinatal lethality and severe skeletal developmental abnormalities as a result of impaired cartilage/bone development and defective growth plate angiogenesis (12). The function of CTGF in cells of the osteoblastic lineage is not well understood, and the study of the effects of CTGF in these cells has yielded controversial results (6, 11, 13, 14). Down-regulation of CTGF using RNA interference revealed that CTGF may be required for osteoblastogenesis, but overexpression of CTGF or addition of CTGF protein to cells of the osteoblastic lineage were reported to both favor and oppose osteoblastogenesis (4, 6, 11, 13, 14). These observations suggest that different *in vitro* experimental conditions can lead to different interactions between CTGF and osteogenic signals and, as a consequence, to different biological events. Recently, we examined the effect of CTGF overexpression on skeletal cells *in vivo*. Transgenic mice overexpressing CTGF under the control of the osteocalcin promoter exhibited decreased bone formation causing osteopenia (15). Osteoblastic cells from CTGF transgenics exhibited decreased osteoblastogenesis and impaired BMP/Smad, Wnt, and IGF-I signaling. These observations demonstrate that CTGF in excess has the potential to act as a BMP, Wnt, and IGF-I antagonist. However, the consequences of *Ctgf* inactivation on adult skeletal homeostasis have not been defined, because the skeletal developmental phenotype of *Ctgf*-null mice leads to perinatal death (12).

The intent of the present study was to define the function of CTGF in skeletal tissue *in vivo*. For this purpose, we created *Ctgf* global and conditional null mice. In the conditional null model, *Ctgf* was inactivated by Cre recombination directed by either the paired-related homeobox 1 (*Prx1*) enhancer expressed in limb buds at d 10.5 of embryonic life (E10.5) or the osteocalcin promoter expressed at E18.5 in osteoblasts. This approach would allow the inactivation of *Ctgf* in the pre- and perinatal skeleton. The skeletal phenotype of *Ctgf* global and conditional null mice was determined by histomorphometric and structural analyses.

Materials and Methods

Generation of *Ctgf*-null mice

To generate a conditional null allele of *Ctgf*, we applied a conditional-by-inversion (COIN) approach using Velocigene (16). Briefly, a bacterial artificial chromosome (BAC) containing mouse genomic DNA encompassing *Ctgf* was selected from a BAC library of 129/SvJ mouse genomic DNA (id 460d11) containing approximately 170 kb of mouse genomic DNA. The *COIN* intron was introduced into exon 2 of *Ctgf* to generate the BAC-based targeting vector for the $Ctgf^{e2COIN}$ allele (Fig. 1). In this process, exon 2 (223 bp) of *Ctgf* is split into two exons so that the 5′ end of exon 2 to the *COIN* intron is 120 bp, and the 3′ end of exon 2 to the *COIN* intron is 103 bp (Fig. 1). This modification does not disrupt expression of *Ctgf* as evidenced by the fact that $Ctgf^{e2COIN/e2COIN}$ mice express *Ctgf* mRNA. The *COIN* intron is a modified intron derived from intron 2 of the rabbit β-globin gene. The *COIN* element contains a *lox66_SA-egfp)-polyA_lox71* sequence placed in the antisense strand, where SA is the 5′ spliced region from rabbit β-globin intron 2 and *polyA* is from the 3′ untranslated region of the rabbit β-globin gene. The *SA-EGFP-polyA* cassette was optimized to block transcription when brought into the sense strand after Cre recombination. The *COIN* element also contained the selection cassette hygromycin phosphotransferase-Δ thymidine kinase mini gene (*HygΔTK*), which was used for the initial selection of embryonic stem (ES) cells and was flanked by flippase (FLP) recognition targets for its removal (17, 18). Conversion of a *COIN* allele from silent to a null allele is brought about by the Cre recombinase that recognizes left/right mutant *lox* sites *lox71* and *lox66* (19, 20). Because *lox66* is in the reverse complement orientation with respect to *lox71*, upon exposure to the enzyme, the *lox66* site recombines with the *lox71* site, inverting the *COIN* sequence flanked by these sites (21). Within the *COIN* element, the *lox66* and *lox71* sites were engineered in a configuration enabling the permanent inversion of the *loxP* flanked sequences by Cre recombinase (22, 23). After inversion, the transcriptional machinery does not access exons 2–5 of *Ctgf*, resulting in a message comprised of exons 1, a fraction of exon 2, and *eGFP*, containing minimal *Ctgf* coding sequences. This should result in the inactivation of *Ctgf* because CTGF is not active in conventional *Ctgf*-null mice containing an intact exon 2 (24).

Using restriction mapping, it was determined that the modified BAC had homology arms of approximately 120 and 40 kb flanking the *COIN* intron, and it was used as a vector to target *Ctgf* in a C57BL/6-129SvJ hybrid ES line, F1H4 286A-B8, that already harbors a null allele of *Ctgf* (24). ES cell clones were genotyped using a loss-of-allele assay, and 12 of 192 clones screened were targeted, indicating a targeting frequency of 6.25%. Targeted ES cell lines were used to generate chimeric male mice at the transgenic facility of the University of Connecticut Health Center (Farmington, CT). Chimeras that were complete transmitters of ES-derived sperm were bred to 129/SvJ mice expressing the FLP recombinase under the control of the Gt(ROSA)26Sor promoter (The Jackson Laboratory, Bar Harbor, ME) for the removal of the *HygΔTK* selection cassette (17, 18). The excision of the selection cassette was confirmed by PCR, and the resulting FLP recombinase transgene was segregated by mating the mice with C57BL/6 wild-type mice. Heterozygous mice were intermated to create homozygous $Ctgf^{e2COIN/e2COIN}$ mice in a 129SvJ/C57BL/6 genetic background.

To study the consequences of the *Ctgf* inactivation during early limb development, $Ctgf^{e2COIN/e2COIN}$ mice were bred to homozygous *Prx1-Cre* mice in a C57BL/6 genetic background (The Jackson Laboratory) to create heterozygous *Prx1-Cre*/+; $Ctgf^{e2COIN/+}$ mice (25). These were mated with $Ctgf^{e2COIN/e2COIN}$ mice to create *Prx1-Cre*/+;$Ctgf^{e2COIN/e2COIN}$ to be mated with $Ctgf^{e2COIN/e2COIN}$ to generate an experimental cohort, in which the *COIN* element is inverted by Cre ($Ctgf^{INV/INV}$) and a control group without Cre-mediated inversion ($Ctgf^{e2COIN/e2COIN}$) and

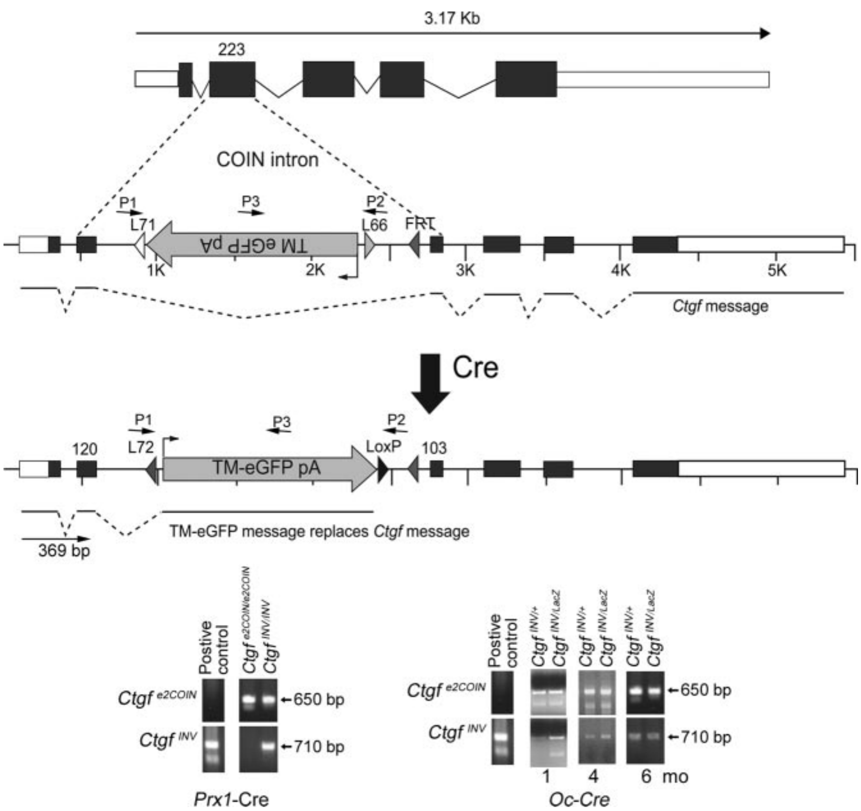

FIG. 1. Engineering of the $Ctgf^{e2COIN}$ allele and strategy for the conditional inactivation of *Ctgf*. The *upper panel* reveals the exon and intron structure of *Ctgf* (adapted from Ensembl.org). *Dark gray boxes* indicate coding sequences, whereas *white boxes* indicate untranslated regions (UTR). The introns are shown as *dotted lines*. In the $Ctgf^{e2COIN}$ allele, exon 2 (223 bp) is split by inserting a *COIN* intron into two new exons of 120 and 103 bp upstream and downstream of the *COIN* intron, respectively. The *COIN* intron contains a *COIN* element that is comprised of *lox66_SA-Egpf-polyA_lox71*, placed in the antisense orientation with respect to the transcription of the *Ctgf*. A single FLP recognition target (FRT) site indicates the placement of the *Hyg*Δ*TK* drug selection cassette, which was removed by the action of FLP. A normal CTGF mRNA is expressed by the $Ctgf^{e2COIN}$ allele. The *middle panel* shows that exposure to Cre recombinase results in the virtually irreversible inversion of the *COIN* element and conversion of the *lox66-lox71* pair to *lox71-loxP*. A new message is expressed, comprised of exons 1, the new exon 2, and *COIN* element exon, which encodes for a transmembrane domain-eGFP fusion protein (TMeGFP). In the *lower panel*, a representative PCR analysis, using primers 1, 2, and 3 (P1, P2, and P3) depicted in the *upper* and *middle panels* and described in Supplemental Table 1, is shown. Calvarial DNA from *Ctgf* conditional null and control mice before and after recombination by Cre expressed under the control of the *Prx1* enhancer (*left panel*) or of the osteocalcin promoter (*right panel*) is shown. A 710-bp band is detected in the $Ctgf^{INV}$ allele, and a 650-bp band is detected in the noninverted allele.

studied at 1 month of age. $Ctgf^{e2COIN/e2COIN}$ mice also were compared with wild-type littermate controls to ensure that before recombination they did not exhibit a skeletal phenotype. To study the inactivation of *Ctgf* in mature osteoblasts, transgenic mice expressing the Cre recombinase under the control of a 3.9-kb human osteocalcin promoter (*Oc-Cre*), created in a Friend virus B type (FVB) genetic background, were obtained from T. Clemens (Baltimore, MD) (26). $Ctgf^{e2COIN/e2COIN}$ mice were studied in a *Ctgf* heterozygous null background. For this purpose, *Oc-Cre* mice were mated to *Ctgf* heterozygous ($Ctgf^{+/LacZ}$) null mice, backcrossed eight times into a C57BL/6 background after the excision of a neomycin selection cassette by breeding with mice expressing the Cre recombinase under the control of the cytomegalovirus (CMV) promoter (24). *Oc-Cre* and *Ctgf* heterozygous mice were intermated for the creation of *Oc-Cre*/*Oc-Cre* homozygous mice in a heterozygous $Ctgf^{+/LacZ}$ null background. These were mated with homozygous $Ctgf^{e2COIN/e2COIN}$ mice, generating an experimental cohort, where Cre inverts the *COIN* element from the $Ctgf^{e2COIN}$ allele and where a *Ctgf*-null allele is retained ($Ctgf^{INV/LacZ}$), and a control littermate cohort is carrying a Cre-inverted $Ctgf^{e2COIN}$ allele and a wild-type allele ($Ctgf^{INV/+}$). To ensure that the latter were appropriate controls, the skeletal phenotype of $Ctgf^{+/LacZ}$ mice was compared with that of wild-type littermate C57BL/6 mice. Conditional null mice were compared with littermate controls of identical genetic composition at 1, 4, and 6 months of age.

Genotyping of *Oc-Cre*, *Prx1-Cre*, $Ctgf^{e2COIN}$, and $Ctgf^{LacZ}$ alleles was carried out by PCR in tail DNA extracts (Supplemental Table 1 published on The Endocrine Society's Journals Online web site at http://endo.endojournals.org). Deletion of the *neo* cassette in $Ctgf^{LacZ}$ mice by Cre recombination and deletion of the *Hyg*Δ*TK* cassette in $Ctgf^{e2COIN/e2COIN}$ mice by FLP recombination was determined by PCR in tail DNA and inversion of *lox71-lox66* flanked sequences in $Ctgf^{e2COIN/e2COIN}$ mice by Cre recombination was documented by PCR in DNA extracted from calvariae (Fig. 1). The *Ctgf*-null state was confirmed by documenting suppressed *Ctgf* mRNA in calvarial extracts by real-time RT-PCR (27, 28). All animal experiments were approved by the Animal Care and Use Committee of Saint Francis Hospital and Medical Center.

X-ray analysis, bone mineral density (BMD), and femoral length

X-rays were performed on eviscerated mice at an intensity of 30 kW for 20 sec on a Faxitron x-ray system (model MX 20; Faxitron X-Ray Corp., Wheeling, IL). Total BMD (grams per square centimeter) was measured on anesthetized mice using the PIXImus small-animal dual-energy x-ray absorptiometry system (GE Medical System/LUNAR, Madison, WI) (29). Femoral images were used to determine femoral length in millimeters. Calibrations were performed with a phantom of defined value, and quality assurance measurements were performed before each use. The coefficient of variation for total BMD is less than 1% (n = 9).

Bone histomorphometric analysis

Static and dynamic histomorphometry was carried out on experimental and control mice after they were injected with calcein (20 mg/kg) and demeclocycline (50 mg/kg) at an interval of 2 d for 1-month-old animals and 7 d for 4- and 6-month-old animals. Mice were killed by CO_2 inhalation 2 d after the demeclocycline injection. Longitudinal sections of femurs, 5 μm thick, were cut on a microtome (Microm; Richards-Allan Scientific, Kalamazoo, MI) and stained with 0.1% toluidine blue or von Kossa. Static parameters of bone formation and resorption were measured in a defined area between 360 and 2160 μm from the growth plate, using an OsteoMeasure morphometry system (Osteometrics, Atlanta, GA) (30). For dynamic histomorphometry, mineralizing surface per bone surface and mineral apposition rate were measured on unstained sections under UV light, using a triple diamidino-2-phenylindole fluorescein set long-pass filter, and bone formation rate was calculated. The terminology and units used are those recommended by the Histomorphometry Nomenclature Committee of the American Society for Bone and Mineral Research (31).

Microcomputed tomography (μCT)

Bone microarchitecture of femurs from experimental and control mice was analyzed by μCT (MicroCT40; Scanco Medical AG, Bassersdorf, Switzerland) (32). The metaphyseal region of the distal femur was scanned for microarchitecture, and cortical thickness was obtained at the midshaft. The femurs were scanned at a resolution of 12 μm, energy level of 45 keV, and intensity of 177 μA. The distal trabecular scan started about 0.6 mm proximal to the growth plate and extended proximally 1.5 mm. One hundred fifty cross-sectional slices were obtained at 12-μm intervals at the distal end beginning at the edge of the growth plate and extending in a proximal direction, and 100 contiguous slices were selected for analysis. Trabecular regions were assessed for bone volume fraction (bone volume/total volume), trabecular thickness, trabecular number, trabecular separation, connectivity density, and structure model index. The midshaft cortical thickness values were obtained by averaging 18 slices at the midpoint of the femur.

Serum C-terminal cross-linked telopeptide of type I collagen (CTX)

The serum bone remodeling marker CTX was measured by ELISA using RatLaps ELISA kits (Nordic Bioscience Diagnostics, Herlev, Denmark), according to manufacturer's instructions.

Primary osteoblast cell cultures and adenoviral infection

Osteoblastic cells were isolated from parietal bones of 3- to 5-d-old *Ctgf*$^{e2COIN/e2COIN}$ mice. Cells were obtained by five sequential digestions of the parietal bones using bacterial collagenase (CLS II; Worthington Biochemical, Freehold, NJ) (33). Cell populations harvested from the third to the fifth digestions were cultured as a pool and were previously shown to have osteoblast characteristics. Osteoblastic cells were cultured in DMEM (Life Technologies, Inc., Grand Island, NY) supplemented with nonessential amino acids, 20 mM HEPES, 100 μg/ml ascorbic acid, and 10% fetal bovine serum (FBS) (Atlanta Biologicals, Lawrenceville, GA) at 37 C in a humidified 5% CO_2 incubator. Subconfluent *Ctgf*$^{e2COIN/e2COIN}$ cells were trypsinized and plated at a density of 25,000 cells/cm^2 and cultured to subconfluence (~35,000 cells/cm^2). Cells were transferred to DMEM containing 2% FBS and transduced with 100 multiplicity of infection of replication-defective recombinant adenovirus. An adenoviral vector expressing Cre recombinase under the control of the CMV promoter (Ad-CMV-Cre; Vector Biolabs, Philadelphia, PA) was used to induce recombination of *lox* sequences *in vitro*, and an adenoviral vector expressing green fluorescent protein (GFP) under the control of the CMV promoter (Ad-CMV-GFP) was used as a control (34). After 24 h, cells were washed with versene (Invitrogen, Carlsbad, CA), trypsinized, plated, and cultured in DMEM containing 10% FBS. *Ctgf* and alkaline phosphatase mRNA were measured by real-time RT-PCR. Alkaline phosphatase activity was determined in 0.5% Triton X-100 cell extracts by the hydrolysis of *p*-nitrophenol phosphate to *p*-nitrophenol and measured by spectroscopy at 405 nm after 10 min of incubation at room temperature according to manufacturer's instructions (Sigma-Aldrich, St. Louis, MO). Data are expressed as nanomoles of *p*-nitrophenol released per minute per microgram of protein. Total protein content was determined in cell extracts by the DC protein assay, in accordance with manufacturer's instructions (Bio-Rad, Hercules, CA).

Real-time RT-PCR

Total RNA was extracted from calvariae or from osteoblast cultures and mRNA levels determined by real-time RT-PCR (27,

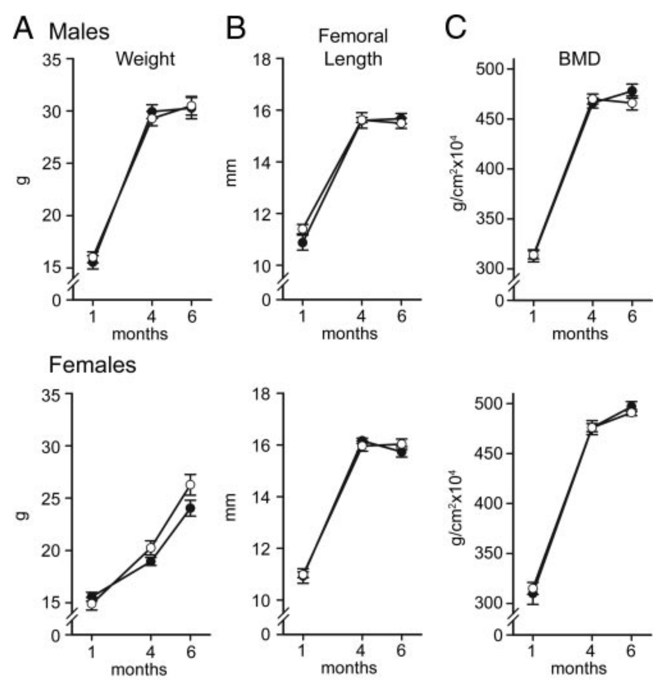

D *Ctgf* mRNA

	Males		Females	
	Wild Type	*Ctgf* $^{+/LacZ}$	Wild Type	*Ctgf* $^{+/LacZ}$
1 month	100 ± 24	51 ± 13	100 ± 16	66 ± 19
4 month	100 ± 11	44 ± 7 *	100 ± 46	31 ± 23
6 month	100 ± 30	21 ± 3 *	100 ± 2	82 ± 29

FIG. 2. Weight, femoral length, BMD, and *Ctgf* mRNA expression in male (*upper panels*) and female (*lower panels*) *Ctgf* $^{+/LacZ}$ heterozygous null mice (●) and wild-type littermate controls (○). The weight in grams (A), femoral length in millimeters (B), total BMD in grams per square centimeter (C), and *Ctgf* mRNA levels in total calvarial extracts (D), expressed as *Ctgf* copy number corrected for *Rpl38* and normalized to 100 at 1, 4, and 6 months of age, are shown. Values are means ± SEM (n = 5–17) except for mRNA levels, which are expressed as percentage of control for each independent age (n = 3–4).
* Significantly different from control mice, $P < 0.05$.

TABLE 1. Femoral histomorphometry of 1-, 4-, and 6-month-old male and female *Ctgf* $^{+/LacZ}$ heterozygous mice and wild-type controls

	1 month		4 months		6 months	
	Wild type	***Ctgf*** $^{+/LacZ}$	**Wild type**	***Ctgf*** $^{+/LacZ}$	**Wild type**	***Ctgf*** $^{+/LacZ}$
Males						
Bone volume/tissue volume (%)	7.7 ± 0.7	5.2 ± 0.6[a]	9.2 ± 0.7	7.7 ± 0.8	7.1 ± 1.1	6.7 ± 1.1
Trabecular separation (μm)	292 ± 25	482 ± 70[a]	252 ± 19	266 ± 13	409 ± 51	372 ± 33
Trabecular number (mm^{-1})	3.4 ± 0.2	2.5 ± 0.2[a]	3.7 ± 0.2	3.5 ± 0.2	2.5 ± 0.3	2.6 ± 0.2
Trabecular thickness (μm)	22.2 ± 1.0	20.8 ± 0.6	24.7 ± 0.6	23.2 ± 0.6	27.4 ± 1.7	25.4 ± 2.6
Osteoblast surface/bone surface (%)	24.5 ± 1.1	25.9 ± 1.5	16.4 ± 1.5	18.4 ± 1.4	15.5 ± 1.2	14.2 ± 0.6
Number of osteoblasts/bone perimeter (mm^{-1})	27 ± 1	30 ± 2	13.3 ± 1.4	15.0 ± 1.1	11.9 ± 1	11.1 ± 1
Number of osteoblasts/tissue area (mm^{-2})	142 ± 9	112 ± 11[a]	77 ± 7	82 ± 5	47 ± 8	45 ± 4
Osteoclast surface/bone surface (%)	16.1 ± 0.6	17.0 ± 0.6	4.4 ± 0.4	4.8 ± 0.5	5.2 ± 0.4	5.6 ± 0.5
Number of osteoclasts/bone perimeter (mm^{-1})	7.3 ± 0.3	8.2 ± 0.2	2.1 ± 0.2	2.3 ± 0.2	2.2 ± 0.1	2.5 ± 0.2
Number of osteoclasts/tissue area (mm^{-2})	43 ± 3	32 ± 3[a]	12 ± 1	13 ± 2	9 ± 1	10 ± 1
Eroded surface/bone surface (%)	28 ± 1	29 ± 1	10 ± 1	11 ± 1	10 ± 1	11 ± 1
Mineral apposition rate (μm/d)	2.20 ± 0.11	2.38 ± 0.09	0.77 ± 0.04	0.85 ± 0.04	0.64 ± 0.03	0.70 ± 0.04
Mineralizing surface/bone surface (%)	1.86 ± 0.35	2.56 ± 0.28	3.69 ± 0.55	3.73 ± 0.49	3.43 ± 0.63	3.15 ± 0.91
Bone formation rate ($\mu m^3/\mu m^2$/d)	0.043 ± 0.009	0.061 ± 0.007	0.029 ± 0.005	0.032 ± 0.005	0.023 ± 0.004	0.023 ± 0.007
Females						
Bone volume/tissue volume (%)	7.1 ± 0.6	4.0 ± 0.8[a]	3.1 ± 3.3	3.3 ± 0.3	3.0 ± 0.4	3.2 ± 0.4
Trabecular separation (μm)	273 ± 31	468 ± 69[a]	695 ± 62	631 ± 54	752 ± 97	704 ± 81
Trabecular number (mm^{-1})	3.6 ± 0.3	2.3 ± 0.4[a]	1.5 ± 0.2	1.6 ± 0.1	1.4 ± 0.2	1.4 ± 0.1
Trabecular thickness (μm)	19.9 ± 0.8	17.2 ± 1.2	19.8 ± 0.4	20.1 ± 0.9	21.5 ± 0.7	21.7 ± 1.1
Osteoblast surface/bone surface (%)	27.7 ± 1.7	27.3 ± 2.1	23.3 ± 2.1	17.8 ± 2.2	26.6 ± 3.2	21.0 ± 1.6
Number of osteoblasts/bone perimeter (mm^{-1})	31 ± 1	32 ± 3	20 ± 2	14 ± 2	19.7 ± 2.5	16.0 ± 1.1
Number of osteoblasts/tissue area (mm^{-2})	171 ± 14	110 ± 10[a]	47 ± 5	34 ± 3[a]	41 ± 5	36 ± 5
Osteoclast surface/bone surface (%)	16.0 ± 0.9	15.6 ± 0.7	8.4 ± 0.6	9.7 ± 0.5	6.8 ± 0.7	7.4 ± 1.4
Number of osteoclasts/bone perimeter (mm^{-1})	8.0 ± 0.4	7.9 ± 0.4	4.3 ± 0.3	4.9 ± 0.3	2.8 ± 0.3	3.2 ± 0.7
Number of osteoclasts/tissue area (mm^{-2})	44 ± 3	28 ± 5[a]	10 ± 1	12 ± 1	6 ± 1	7 ± 1
Eroded surface/bone surface (%)	29 ± 2	29 ± 1	18 ± 1	22 ± 0	13 ± 1	15 ± 3
Mineral apposition rate (μm/d)	2.12 ± 0.14	2.13 ± 0.36	1.01 ± 0.11	1.14 ± 0.07	1.11 ± 0.04	1.14 ± 0.07
Mineralizing surface/bone surface (%)	3.9 ± 0.6	3.8 ± 0.5	1.84 ± 0.40	1.57 ± 0.29	6.68 ± 1.61	10.55 ± 1.03
Bone formation rate ($\mu m^3/\mu m^2$/d)	0.084 ± 0.014	0.080 ± 0.009	0.019 ± 0.004	0.018 ± 0.003	0.076 ± 0.020	0.118 ± 0.009

Bone histomorphometry was performed on femurs from 1-, 4-, and 6-month-old male and female C*tgf* $^{+/LacZ}$ heterozygous mice and wild-type littermate controls. Values are means ± SEM (n = 5–13).

[a] Significantly different from controls, $P < 0.05$ by unpaired *t* test.

28). For this purpose, RNA was reverse transcribed using SuperScript III Platinum Two-Step qRT-PCR kit (Invitrogen), according to manufacturer's instructions. Product amplification was conducted in the presence of 5′-CACTCCGGGAAATGCTGCAAGGAG[FAM]G-3′ and 5′-GTTGGGTCTGGGCCAAATGT-3′ primers for CTGF (GenBank accession number NM_010217), which binds at base 772 and 840 of the CTGF reverse-transcribed DNA; 5′-CGGTTAGGGCGTCTCCACAGTAAC[FAM]G-3′ and 5′-CTTGGAGAGGGCCACAAAGG-3′ primers for alkaline phosphatase (GenBank accession no. NM_007431), which binds at base 439 and 514 of the alkaline phosphatase reverse-transcribed DNA; and 5′-CGAACCGGATAATGTGAAGTTCAAGGTT[FAM]G-3′ and 5′-CTGCTTCAGCTTCTCTGCCTTT-3′ primers for ribosomal protein L38 (RPL38) (GenBank accession no. NM_001048057), which binds at base 223 and 268 of the RPL38 reverse-transcribed DNA. Primers were mixed with Platinum Quantitative PCR SuperMix-UDG (Invitrogen) and amplification conducted at 60 C for 45 cycles (35). Transcript copy number was estimated by comparison with a standard curve constructed using CTGF (R. P. Rysek, Princeton, NJ), alkaline phosphatase, or RPL38 (both from American Type Culture Collection, Manassas, VA) cDNA (36). Reactions were conducted in a 96-well spectrofluorometric thermal iCycler (Bio-Rad), and fluorescence was monitored during every PCR cycle at the annealing step. Data are expressed as copy number corrected for *Rpl38*.

Statistical analysis

Data are expressed as means ± SEM. Statistical differences were determined by unpaired Student's *t* test or ANOVA.

Results

Ctgf heterozygous null mice

To study *Ctgf* heterozygous null mice, *Ctgf* $^{+/LacZ}$ mice were mated with wild-type mice to obtain *Ctgf* $^{+/LacZ}$ mice and wild-type littermate controls. *Ctgf* mRNA levels were 20–80% lower in calvariae from 1-, 4-, and 6-month-old *Ctgf* $^{+/LacZ}$ than in calvarial extracts from wild-type controls (Fig. 2). *Ctgf* $^{+/LacZ}$ heterozygous null mice appeared normal and not different from their wild-type littermates. Contact radiography at 1, 4, and 6 months of age revealed no apparent skeletal abnormalities in *Ctgf* $^{+/LacZ}$ mice (not shown). *Ctgf* $^{+/LacZ}$ heterozygous null mice had normal body weight, femoral length, and BMD at 1, 4, and 6 months of age (Fig. 2). Static and dynamic histomorphometric analysis revealed a 30–45% decrease in bone volume/tissue volume at 1 month of age in male and female *Ctgf* $^{+/LacZ}$ mice (Table 1 and Fig. 3). In accordance with the endochondral skeletal developmental phenotype of homozygous *Ctgf*-null mice, the osteopenia appeared to be secondary to a decreased num-

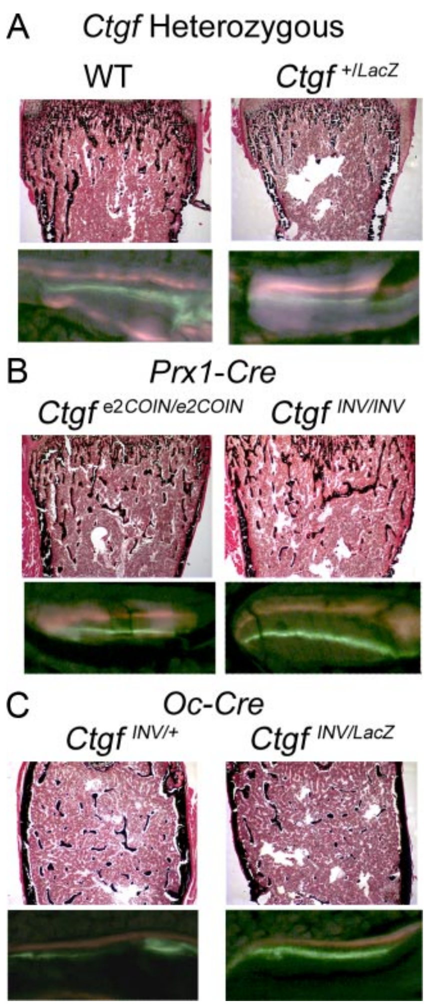

FIG. 3. Representative histological sections and calcein/demeclocycline labeling of bone femoral sections from 1-month-old *Ctgf* $^{+/LacZ}$ heterozygous mice (A), 1-month-old *Prx1-Cre*/+;*Ctgf* $^{INV/INV}$ conditional null mice and littermate *Ctgf* $^{e2COIN/e2COIN}$ controls (B), and 6-month-old *Oc-Cre*/+;*Ctgf* $^{INV/LacZ}$ conditional null mice and *Oc-Cre*/+;*Ctgf* $^{INV/+}$ littermate controls (C). Sections from male mice were stained with von Kossa without counterstain (final magnification, ×40) or unstained and examined under fluorescence microscopy (final magnification, ×400). WT, Wild type.

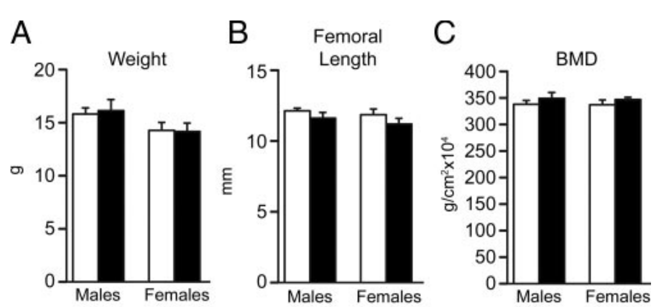

D *Ctgf* mRNA

Males		Females	
Ctgf $^{e2COIN/e2COIN}$	*Ctgf* $^{INV/INV}$	*Ctgf* $^{e2COIN/e2COIN}$	*Ctgf* $^{INV/INV}$
100 ± 18	57 ± 17	100 (n=2)	48 ± 15

FIG. 4. Weight, femoral length, BMD, and *Ctgf* expression in male and female *Prx1-Cre*/+;*Ctgf* $^{INV/INV}$ conditional null mice (*black bars*) and littermate *Ctgf* $^{e2COIN/e2COIN}$ controls (*white bars*). The weight in grams (A), femoral length in millimeters (B), total BMD in grams per square centimeter (C), and *Ctgf* mRNA levels in total calvarial extracts (D), expressed as *Ctgf* copy number corrected for *Rpl38* and normalized to 100, are shown. Values are means ± SEM (n = 3–6), except for RNA levels, which are expressed as percentage of control (n = 2–6).

ber of trabeculae by 27% in male and 36% in female mice ($P < 0.05$). Trabecular thickness was not decreased significantly (6–14%), and the osteopenia was transient and not observed in 4- or 6-month-old *Ctgf* $^{+/LacZ}$ heterozygous mice. Osteoblast and osteoclast number per perimeter and parameters of bone formation or bone resorption were not different between *Ctgf* $^{+/LacZ}$ and wild-type controls at 1–6 months of age.

Conditional *Ctgf*-null mice

To induce the conditional inactivation of *Ctgf* in the limb bud at E10.5, *Prx1-Cre/+;Ctgf* $^{e2COIN/e2COIN}$ mice were mated with *Ctgf* $^{e2COIN/e2COIN}$ mice to create limb bud-specific *Prx1-Cre/+;Ctgf* $^{INV/INV}$ conditional null and *Ctgf* $^{e2COIN/e2COIN}$ to serve as littermate controls (25). In preliminary experiments, we documented that *Ctgf* $^{e2COIN/e2COIN}$ mice were not different from wild-type controls by bone histomorphometric analysis (not shown). *Ctgf* mRNA levels in calvarial extracts from conditional *Prx1-Cre/+;Ctgf* $^{INV/INV}$-null mice were about 50% lower than in control mice (Fig. 4). The conditional inactivation of *Ctgf* in the developing limb bud caused a similar phenotype as that described for heterozygous *Ctgf* $^{+/LacZ}$ mice at 1 month of age. Conditional *Prx1-Cre/+;Ctgf* $^{INV/INV}$ mice appeared normal; their weight, femoral length, and BMD were not different from controls (Fig. 4), and contact radiography did not reveal skeletal abnormalities (not shown). Bone histomorphometric analysis revealed osteopenia secondary to decreased trabecular number in male, but not in female, mice, suggesting impaired formation of bone trabeculae during development (Table 2 and Fig. 3). The number of osteoblasts and osteoclasts in conditional *Prx1-Cre/+;Ctgf* $^{INV/INV}$-null mice were not different from control mice, and eroded surface and bone formation were not affected. Serum levels of the marker of bone remodeling CTX were not different between *Ctgf* conditional null mice and controls (not shown). μCT revealed a 25% decrease in trabecular bone volume in male *Ctgf* conditional null mice, but that decrease was not statistically significant, and other parameters of bone structure were not affected (Supplemental Table 2).

For the conditional deletion of *Ctgf* in mature osteoblasts, *Oc-Cre/Oc-Cre;Ctgf* $^{+/LacZ}$ were mated with homozygous

TABLE 2. Femoral histomorphometry of 1-month-old male and female *Prx1-Cre/+;Ctgf* $^{INV/INV}$ conditional null mice and controls

	Ctgf $^{e2COIN/e2COIN}$	***Ctgf*** $^{INV/INV}$
Males		
Bone volume/tissue volume (%)	13.2 ± 1.2	9.2 ± 0.8[a]
Trabecular separation (μm)	189 ± 15	250 ± 18[a]
Trabecular number (mm^{-1})	4.7 ± 0.3	3.7 ± 0.2[a]
Trabecular thickness (μm)	27.7 ± 1.7	24.6 ± 1.2
Osteoblast surface/bone surface (%)	36.2 ± 2.5	35.9 ± 1.8
Number of osteoblasts/bone perimeter (mm^{-1})	36.5 ± 2.3	37.4 ± 2.5
Number of osteoblasts/tissue area (mm^{-2})	272 ± 26	221 ± 24
Osteoclast surface/bone surface (%)	10.8 ± 0.7	10.1 ± 0.8
Number of osteoclasts/bone perimeter (mm^{-1})	5.2 ± 0.3	4.8 ± 0.3
Number of osteoclasts/tissue area (mm^{-2})	39 ± 3	28 ± 2[a]
Eroded surface/bone surface (%)	23 ± 2	21 ± 1
Mineral apposition rate (μm/d)	3.33 ± 0.18	3.35 ± 0.11
Mineralizing surface/bone surface (%)	1.67 ± 0.28	3.52 ± 1.17
Bone formation rate ($\mu m^3/\mu m^2/d$)	0.055 ± 0.009	0.123 ± 0.042
Females		
Bone volume/tissue volume (%)	10.2 ± 0.6	9.7 ± 1.1
Trabecular separation (μm)	293 ± 12	309 ± 26
Trabecular number (mm^{-1})	3.1 ± 0.1	3.0 ± 0.2
Trabecular thickness (μm)	33.2 ± 0.8	31.6 ± 1.1
Osteoblast surface/bone surface (%)	36.1 ± 2.1	32.8 ± 1.4
Number of osteoblasts/bone perimeter (mm^{-1})	34.2 ± 0.9	33.4 ± 1.2
Number of osteoblasts/tissue area (mm^{-2})	210 ± 2	202 ± 17
Osteoclast surface/bone surface (%)	7.1 ± 0.1	8.0 ± 0.6
Number of osteoclasts/bone perimeter (mm^{-1})	4.4 ± 0.3	5.2 ± 0.4
Number of osteoclasts/tissue area (mm^{-2})	27 ± 2	31 ± 3
Eroded surface/bone surface (%)	19 ± 2	22 ± 1
Mineral apposition rate (μm/d)	4.01 ± 0.13	3.95 ± 0.21
Mineralizing surface/bone surface (%)	1.33 ± 0.42	1.84 ± 0.45
Bone formation rate ($\mu m^3/\mu m^2/d$)	0.052 ± 0.015	0.071 ± 0.015

Bone histomorphometry was performed on femurs from 1-month-old male and female *Prx1-Cre/+;Ctgf* $^{INV/INV}$ conditional null mice and *Ctgf* $^{e2COIN/e2COIN}$ littermate controls. Values are means ± SEM (n = 6–7).

[a] Significantly different from controls, $P < 0.05$ by unpaired *t* test.

Ctgf$^{e2COIN/e2COIN}$ mice to create *Oc-Cre*/+;*Ctgf*$^{INV/LacZ}$ as an experimental group and *Oc-Cre*/+;*Ctgf*$^{INV/+}$ as littermate controls. CTGF mRNA levels in calvarial extracts from *Oc-Cre*/+;*Ctgf*$^{INV/LacZ}$ conditional null mice were suppressed by 60–90% in relation to those measured in littermate controls. Although heterozygous *Ctgf*$^{+/LacZ}$ mice had an osteopenic phenotype at 1 month of age (Table 1), it was transient and not observed at 4 and 6 months of age. Consequently, heterozygous *Oc-Cre*/+;*Ctgf*$^{INV/+}$ mice were considered to be comparable to wild-type mice at 4 and 6 months of age. When compared with heterozygous *Oc-Cre*/+;*Ctgf*$^{INV/+}$ littermates, *Oc-Cre*/+;*Ctgf*$^{INV/LacZ}$ conditional null mice appeared visually normal and had normal weight, femoral length, and BMD (Fig. 5), and contact radiography did not reveal obvious skeletal abnormalities (not shown). Although 1-month-old heterozygous *Ctgf*$^{+/LacZ}$ mice were osteopenic compared with wild-type mice, removal of a second allele in conditional

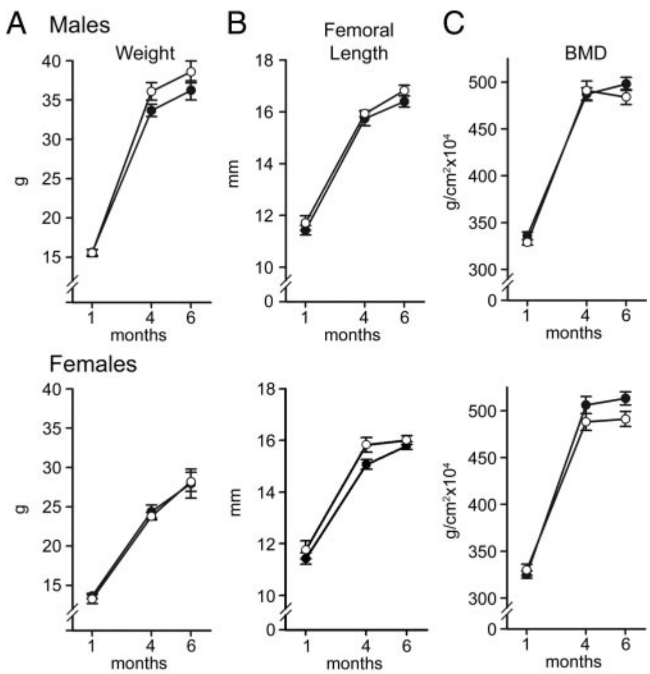

D *Ctgf* mRNA

	Males		Females	
	Ctgf $^{INV/+}$	*Ctgf* $^{INV/LacZ}$	*Ctgf* $^{INV/+}$	*Ctgf* $^{INV/LacZ}$
1 month	100 ± 30	11 ± 3 *	100 (n=2)	11 ± 4
4 month	100 ± 29	42 ± 11	100 ± 17	29 ± 8 *
6 month	100 ± 14	11 ± 3 *	100 ± 37	37 ± 22

FIG. 5. Weight, femoral length, BMD, and *Ctgf* expression in male (*upper panels*) and female (*lower panels*) *Oc-Cre*/+;*Ctgf*$^{INV/LacZ}$ conditional null mice (●) and *Oc-Cre*/+;*Ctgf*$^{INV/+}$ littermate controls (○). The weight in grams (A), femoral length in millimeters (B), total BMD in grams per square centimeter (C), and *Ctgf* mRNA levels in total calvarial extracts (D), expressed as *Ctgf* copy number corrected for *Rpl38* and normalized to 100 at 1, 4, and 6 months of age, are shown. Values are means ± SEM (n = 4–13) except for mRNA levels, which are expressed as percentage of control for each independent age (n = 2–6). *, Significantly different from controls by unpaired *t* test, $P < 0.05$.

Oc-Cre/+;*Ctgf*$^{INV/LacZ}$ mice did not accentuate the phenotype (Table 3). Female 1-month-old conditional *Ctgf*-null mice exhibited decreased trabecular separation, but bone volume was not significantly affected. Bone histomorphometric analysis of femurs from 4-month-old male and female *Oc-Cre*/+;*Ctgf*$^{INV/LacZ}$ conditional null mice revealed no skeletal phenotype when compared with *Oc-Cre*/+;*Ctgf*$^{INV/+}$ mice (Table 3 and Fig. 3). A decrease in trabecular bone volume was observed at 6 months of age in male *Oc-Cre*/+;*Ctgf*$^{INV/LacZ}$-null mice. The decrease in bone volume was secondary to a decrease in trabecular number. Osteoblast number/perimeter and osteoblast surface were not different from controls. Fluorescence microscopy of *Oc-Cre*/+;*Ctgf*$^{INV/LacZ}$ conditional null male and female mice did not reveal changes in bone formation rate. Changes in trabecular bone volume in 6-month-old male mice were not associated with changes in bone resorption, because osteoclast number and eroded surface were normal, and serum CTX levels were not different from control mice (not shown). μCT of *Oc-Cre*/+;*Ctgf*$^{INV/LacZ}$ revealed microarchitectural changes in male mice consistent with the histomorphometric data (Table 4). Bone volume and trabecular number were decreased, and connectivity was reduced by 70%. The changes affected the trabecular compartment only, and cortical thickness was not different between *Oc-Cre*/+;*Ctgf*$^{INV/LacZ}$ and controls.

Inactivation of *Ctgf* in osteoblast cultures

To investigate the consequences of the *Ctgf* inactivation *in vitro*, calvarial osteoblasts from *Ctgf*$^{e2COIN/e2COIN}$ mice were cultured and transduced either with Ad-CMV-Cre to ablate *Ctgf* or with Ad-CMV-GFP as a control. Ad-CMV-Cre decreased the expression of *Ctgf* mRNA by 50–70% in cultured osteoblasts, and down-regulation of *Ctgf* resulted in decreased expression of alkaline phosphatase mRNA and alkaline phosphatase activity, suggesting that CTGF is required for normal osteoblastic function (Supplemental Table 3).

Discussion

Our findings demonstrate that heterozygous *Ctgf*-null mice survive postnatally and confirm that *Ctgf* is required for normal skeletal development because *Ctgf* haploinsufficiency caused reduced trabecular number (12). However, *Ctgf* haploinsufficiency did not appear to influence postnatal growth beyond 1 month of age, because the skeletal phenotype observed at 1 month resolves at 4 months of age. The skeletal phenotype of heterozygous *Ctgf*-null mice was reproduced by the conditional inactivation of

TABLE 3. Femoral histomorphometry of 1-, 4-, and 6-month-old male and female *Oc-Cre/+;Ctgf* $^{INV/LacZ}$ conditional null mice and controls

	1 Month		4 Months		6 Months	
	Ctgf $^{INV/+}$	*Ctgf* $^{INV/LacZ}$	*Ctgf* $^{INV/+}$	*Ctgf* $^{INV/LacZ}$	*Ctgf* $^{INV/+}$	*Ctgf* $^{INV/LacZ}$
Males						
Bone volume/tissue volume (%)	10.0 ± 1.4	9.2 ± 1.0	7.6 ± 1.2	6.4 ± 0.7	8.3 ± 0.8	5.4 ± 0.6[a]
Trabecular separation (μm)	205 ± 27	234 ± 27	328 ± 51	347 ± 26	305 ± 21	444 ± 43[a]
Trabecular number (mm^{-1})	4.6 ± 0.6	4.3 ± 0.4	3.0 ± 0.4	2.8 ± 0.2	3.1 ± 0.2	2.3 ± 0.2[a]
Trabecular thickness (μm)	21.7 ± 1.4	21.6 ± 0.6	25.1 ± 1.7	22.8 ± 1.2	26.6 ± 1.6	23.4 ± 1.2
Osteoblast surface/bone surface (%)	22.4 ± 1.8	20.2 ± 1.3	12.6 ± 0.9	13.4 ± 1.2	15.0 ± 1.8	18.1 ± 1.0
Number of osteoblasts/bone perimeter (mm^{-1})	24.4 ± 2.5	22.0 ± 1.5	12.2 ± 0.8	13.5 ± 1.0	11.9 ± 1.4	15.0 ± 1.1
Number of osteoblasts/tissue area (mm^{-2})	183 ± 40	145 ± 15	58 ± 10	58 ± 5	57 ± 7	52 ± 4
Osteoclast surface/bone surface (%)	13.4 ± 1.6	14.4 ± 0.8	8.4 ± 0.7	9.9 ± 0.7	4.6 ± 0.5	5.2 ± 0.5
Number of osteoclasts/bone perimeter (mm^{-1})	5.9 ± 0.7	6.4 ± 0.4	4.8 ± 0.4	5.5 ± 0.3	2.1 ± 0.2	2.5 ± 0.2
Number of osteoclasts/tissue area (mm^{-2})	41 ± 3	42 ± 4	22 ± 2	24 ± 3	10 ± 1	9 ± 1
Eroded surface/bone surface (%)	21.8 ± 2.0	25.0 ± 1.6	23.2 ± 2.3	25.9 ± 1.1	10.5 ± 1.1	11.6 ± 1.1
Mineral apposition rate (μm/d)	1.93 ± 0.20	1.86 ± 0.09	0.62 ± 0.06	0.50 ± 0.05	0.60 ± 0.03	0.60 ± 0.03
Mineralizing surface/bone surface (%)	2.62 ± 0.60	3.68 ± 0.42	5.35 ± 2.14	3.47 ± 1.35	3.35 ± 0.71	2.08 ± 0.55
Bone formation rate ($\mu m^3/\mu m^2/d$)	0.053 ± 0.017	0.067 ± 0.006	0.03 ± 0.02	0.02 ± 0.01	0.020 ± 0.005	0.013 ± 0.004
Females						
Bone volume/tissue volume (%)	3.8 ± 0.3	5.9 ± 0.7	3.4 ± 0.5	2.5 ± 0.7	1.8 ± 0.4	2.6 ± 0.5
Trabecular separation (μm)	554 ± 32	366 ± 52[a]	662 ± 73	913 ± 167	1188 ± 204	982 ± 237
Trabecular number (mm^{-1})	1.8 ± 0.1	2.8 ± 0.4	1.5 ± 0.2	1.2 ± 0.2	0.9 ± 0.1	1.2 ± 0.2
Trabecular thickness (μm)	21.6 ± 1.1	21.5 ± 0.7	22.2 ± 1.8	19.8 ± 1.5	18.6 ± 1.5	20.9 ± 2.0
Osteoblast surface/bone surface (%)	24.3 ± 3.5	21.8 ± 1.1	16.1 ± 1.5	16.7 ± 4.7	19.1 ± 2.1	16.7 ± 1.7
Number of osteoblasts/bone perimeter (mm^{-1})	25.0 ± 3.8	23.1 ± 1.2	16.2 ± 1.4	15.8 ± 3.8	22.0 ± 2.3	18.9 ± 1.8
Number of osteoblasts/tissue area (mm^{-2})	68 ± 10	102 ± 18	40 ± 7	33 ± 12	33 ± 7	36 ± 6
Osteoclast surface/bone surface (%)	15.4 ± 2.1	15.8 ± 0.7	9.4 ± 0.2	9.8 ± 0.8	13.3 ± 1.7	13.1 ± 0.8
Number of osteoclasts/bone perimeter (mm^{-1})	7.1 ± 1.0	7.0 ± 0.4	6.0 ± 0.2	6.8 ± 0.4	6.8 ± 0.8	6.3 ± 0.4
Number of osteoclasts/tissue area (mm^{-2})	19 ± 3	31 ± 5	14 ± 2	13 ± 3	10 ± 2	12 ± 2
Eroded surface/bone surface (%)	27.9 ± 3.4	25.6 ± 0.9	24.6 ± 0.5	28.6 ± 2.9	21.9 ± 2.5	23.3 ± 1.4
Mineral apposition rate (μm/d)	1.84 ± 0.01	2.14 ± 0.17	0.87 ± 0.05	0.99 ± 0.20	0.66 ± 0.08	0.81 ± 0.06
Mineralizing surface/bone surface (%)	5.09 ± 1.00	2.99 ± 0.19[a]	6.02 ± 0.91	4.43 ± 1.03	12.45 ± 2.96	11.25 ± 1.77
Bone formation rate ($\mu m^3/\mu m^2/d$)	0.094 ± 0.019	0.064 ± 0.007	0.053 ± 0.01	0.035 ± 0.01	0.093 ± 0.031	0.10 ± 0.02

Bone histomorphometry was performed on femurs from 1-, 4-, and 6-month-old male and female *Oc-Cre/+;Ctgf* $^{INV/LacZ}$ conditional null mice and *Oc-Cre/+;Ctgf* $^{INV/+}$ littermate controls. Values are means ± SEM (n = 3–10).

[a] Significantly different from controls, $P < 0.05$ by unpaired *t* test.

TABLE 4. Femoral bone microarchitecture assessed by μCT of 6-month-old male *Oc-Cre/+;Ctgf* $^{INV/LacZ}$ conditional null mice and controls

	Ctgf $^{INV/+}$	*Ctgf* $^{INV/LacZ}$
Bone volume/tissue volume (%)	9.7 ± 2.0	5.9 ± 0.9[b]
Trabecular separation (μm)	221 ± 9	288 ± 13[a]
Trabecular number (mm^{-1})	4.4 ± 0.2	3.5 ± 0.1[a]
Trabecular thickness (μm)	48 ± 2	52 ± 3
Connectivity density ($1/mm^3$)	60.7 ± 14.2	17.2 ± 4.7[a]
Structure model index	3.0 ± 0.2	3.5 ± 0.3
Cortical thickness (μm)	224 ± 4	216 ± 4

Bone μCT was performed on femurs from *Oc-Cre/+;Ctgf* $^{INV/LacZ}$ conditional null mice and *Oc-Cre/+;Ctgf* $^{INV/+}$ littermate controls.

[a] Significantly different from controls, $P < 0.05$ by unpaired *t* test.

[b] $P < 0.057$ by unpaired *t* test.

Ctgf in male mice using the *Prx1* enhancer to direct the Cre recombinase. This is in agreement with the expression of the *Prx1* enhancer at E10.5 in the limb bud (25). The osteopenic phenotype of both the global and the conditional inactivation of *Ctgf* was characterized by a decreased number of bone trabeculae, confirming that CTGF is required for the formation of normal trabeculae and for endochondral bone formation (12). The conditional inactivation of *Ctgf* in the adult skeletal environment was achieved by expressing the Cre recombinase under the control of the osteocalcin promoter. *Ctgf* inactivation caused a decrease in trabecular bone volume secondary to a decrease in the number of trabeculae in older male mice. It is of interest that the conditional deletion of *Ctgf* caused a skeletal phenotype in male, but not in female, mice when directing Cre under either the osteocalcin promoter or the *Prx1* enhancer. There is no immediate explanation for the sexual dimorphism observed in the skeletal phenotype of *Ctgf* conditional null mice, although probably it is due to inherent differences in the skeletal architecture of male and female mice. In this study, we confirm earlier observations demonstrating a more rapid age-dependent decline in trabecular bone volume in C57BL/6 female than in male mice, so that at the same age, the bone architecture differs between the two sexes (32). The lack of a skeletal phenotype at 6 months of age in *Ctgf*-null female mice may be because they have little trabecular bone structure, possibly precluding an additional decrease by the *Ctgf* inactivation. Another alternative is that the Cre recombination is more efficient in skeletal cells from male than from female mice. This does not seem probable because the decrease in skeletal *Ctgf* mRNA levels was not appreciably different between male and female *Ctgf* conditional null mice. The *in vivo* phenotype we describe indicates that CTGF is required not only for skeletal development but also to maintain adult skeletal homeostasis in male mice. Cyr 61, NOV, WISP-1, and WISP-2 are expressed by osteoblasts but did not appear to compensate for the absence of CTGF in the postnatal skeleton of male mice (5).

The osteopenia observed in adult *Ctgf* conditional null male mice is to an extent contradictory to previous work demonstrating that transgenic overexpression of CTGF under the control of the osteocalcin or the type XI collagen promoter causes osteopenia (15, 37). This was secondary to decreased bone formation and interpreted to be secondary to the binding of BMP, Wnt, and IGF-I by CTGF, resulting in decreased activity of these osteogenic signals. A mechanism of action of CTGF entails the inhibition of BMP-2 activity by direct binding of CTGF to BMP-2 (6, 7). Other CCN proteins, such as NOV, appear to act by similar mechanisms, because NOV binds BMPs (38). This is not surprising in view of the structural similarities among CCN proteins, and between CCN proteins and classic BMP antagonists, such as twisted gastrulation and chordin (1–3). Recently, we demonstrated that whereas NOV overexpression causes osteopenia, its global inactivation does not cause an obvious skeletal phenotype (39). These results bear similarities to those obtained in mice misexpressing CTGF and suggest that overexpression of CCN proteins prevent the actions of the osteogenic signals they bind; but until now, CCN proteins appear to be mostly dispensable for skeletal homeostasis. These observations do not exclude an important role of CCN proteins in skeletal homeostasis during conditions of induction. For CTGF, this occurs after BMP signaling and may serve to temper the activity of the osteogenic signal. It is of interest that neither the inactivation nor the overexpression of WISP-3 in an array of tissues caused a phenotype (40, 41).

An expectation of the *Ctgf* inactivation would have been enhanced activity of BMP, Wnt, and IGF-I and, as a consequence, increased bone formation and bone volume. An alternate explanation of the findings is that the *Ctgf* inactivation caused a sensitization to BMP-2 and IGF-I activity and, as a consequence, increased bone resorption (42–45). However, if the phenotype observed in conditional *Ctgf*-null mice was caused by increased BMP and IGF-I activity and bone resorption, this would have been modest and transient because neither histomorphometric parameters nor biochemical markers of bone resorption revealed any differences between experimental and control mice under the conditions of this study.

The *in vivo* phenotype of the conditional inactivation of *Ctgf* also could be due to direct actions of CTGF on skeletal homeostasis. In accordance with this possibility, short-term cultures of *Ctgf* $^{e2COIN/e2COIN}$ osteoblasts where *Ctgf* was inactivated *in vitro* after the transduction of an Ad-CMV-Cre adenoviral vector exhibited decreased alkaline phosphatase expression, suggesting that CTGF is required for normal osteoblastic function. These results are in agreement with previous work in ST-2 stromal cells, where CTGF induces osteoblastogenesis (11). CTGF inhibits Notch signaling in ST-2 stromal cells, and CTGF may be necessary to temper the activity of Notch *in vivo*, a signal that inhibits osteoblastogenesis and causes osteopenia (34, 46). Therefore, in the absence of CTGF, Notch activity may be enhanced and cause the osteopenia observed in *Ctgf*-null male mice. However, there were no changes in osteoblast number or significant changes in bone formation in *Ctgf*-null mice, suggesting that if enhanced Notch signaling was a factor, it played either a transient or a modest role.

In conclusion, our studies reveal that CTGF is necessary for normal skeletal development and postnatal skeletal homeostasis in male, but not female, mice.

Acknowledgments

We thank T. Clemens for Osteocalcin-Cre transgenics; R. P. Rysek for *Ctgf* cDNA; Melissa Burton, Harold Coombs, Deena Durant, Trung X. Le, and Kristen Parker for technical assistance; and Mary Yurczak for secretarial assistance.

Address all correspondence and requests for reprints to: Ernesto Canalis, M.D., Department of Research, Saint Francis Hospital and Medical Center, 114 Woodland Street, Hartford, Connecticut 06105-1299. E-mail: ecanalis@stfranciscare.org.

This work was supported by Grants AR021707 (to E.C.) and AR043618 (to W.B.) from the National Institute of Arthritis and Musculoskeletal and Skin Diseases and Grants DK045227 (to E.C.) and DK042424 (to E.C.) from the National Institute of Diabetes and Digestive and Kidney Diseases.

Disclosure Summary: A.N.E. is employed by Regeneron Pharmaceuticals and owns Regeneron Pharmaceuticals stock. Other authors have nothing to disclose.

References

1. **Brigstock DR** 2003 The CCN family: a new stimulus package. J Endocrinol 178:169–175
2. **Brigstock DR, Goldschmeding R, Katsube KI, Lam SC, Lau LF, Lyons K, Naus C, Perbal B, Riser B, Takigawa M, Yeger H** 2003 Proposal for a unified CCN nomenclature. Mol Pathol 56:127–128
3. **Garcia Abreu J, Coffinier C, Larraín J, Oelgeschläger M, De Robertis EM** 2002 Chordin-like CR domains and the regulation of evolutionarily conserved extracellular signaling systems. Gene 287:39–47
4. **Luo Q, Kang Q, Si W, Jiang W, Park JK, Peng Y, Li X, Luu HH, Luo J, Montag AG, Haydon RC, He TC** 2004 Connective tissue growth factor (CTGF) is regulated by Wnt and bone morphogenetic proteins signaling in osteoblast differentiation of mesenchymal stem cells. J Biol Chem 279:55958–55968
5. **Parisi MS, Gazzerro E, Rydziel S, Canalis E** 2006 Expression and regulation of CCN genes in murine osteoblasts. Bone 38:671–677
6. **Abreu JG, Ketpura NI, Reversade B, De Robertis EM** 2002 Connective-tissue growth factor (CTGF) modulates cell signalling by BMP and TGF-β. Nat Cell Biol 4:599–604
7. **Mercurio S, Latinkic B, Itasaki N, Krumlauf R, Smith JC** 2004 Connective-tissue growth factor modulates WNT signalling and interacts with the WNT receptor complex. Development 131:2137–2147
8. **Song JJ, Aswad R, Kanaan RA, Rico MC, Owen TA, Barbe MF, Safadi FF, Popoff SN** 2007 Connective tissue growth factor (CTGF) acts as a downstream mediator of TGF-β1 to induce mesenchymal cell condensation. J Cell Physiol 210:398–410
9. **Iso T, Kedes L, Hamamori Y** 2003 HES and HERP families: multiple effectors of the Notch signaling pathway. J Cell Physiol 194:237–255
10. **Kopan R, Ilagan MX** 2009 The canonical Notch signaling pathway: unfolding the activation mechanism. Cell 137:216–233
11. **Smerdel-Ramoya A, Zanotti S, Deregowski V, Canalis E** 2008 Connective tissue growth factor enhances osteoblastogenesis in vitro. J Biol Chem 283:22690–22699
12. **Ivkovic S, Yoon BS, Popoff SN, Safadi FF, Libuda DE, Stephenson RC, Daluiski A, Lyons KM** 2003 Connective tissue growth factor coordinates chondrogenesis and angiogenesis during skeletal development. Development 130:2779–2791
13. **Nishida T, Nakanishi T, Asano M, Shimo T, Takigawa M** 2000 Effects of CTGF/Hcs24, a hypertrophic chondrocyte-specific gene product, on the proliferation and differentiation of osteoblastic cells in vitro. J Cell Physiol 184:197–206
14. **Safadi FF, Xu J, Smock SL, Kanaan RA, Selim AH, Odgren PR, Marks Jr SC, Owen TA, Popoff SN** 2003 Expression of connective tissue growth factor in bone: its role in osteoblast proliferation and differentiation in vitro and bone formation in vivo. J Cell Physiol 196:51–62
15. **Smerdel-Ramoya A, Zanotti S, Stadmeyer L, Durant D, Canalis E** 2008 Skeletal overexpression of connective tissue growth factor (CTGF) impairs bone formation and causes osteopenia. Endocrinology 149:4374–4381
16. **Valenzuela DM, Murphy AJ, Frendewey D, Gale NW, Economides AN, Auerbach W, Poueymirou WT, Adams NC, Rojas J, Yasenchak J, Chernomorsky R, Boucher M, Elsasser AL, Esau L, Zheng J, Griffiths JA, Wang X, Su H, Xue Y, Dominguez MG, Noguera I, Torres R, Macdonald LE, Stewart AF, DeChiara TM, Yancopoulos GD** 2003 High-throughput engineering of the mouse genome coupled with high-resolution expression analysis. Nat Biotechnol 21:652–659
17. **Buchholz F, Ringrose L, Angrand PO, Rossi F, Stewart AF** 1996 Different thermostabilities of FLP and Cre recombinases: implications for applied site-specific recombination. Nucleic Acids Res 24:4256–4262
18. **Buchholz F, Angrand PO, Stewart AF** 1998 Improved properties of FLP recombinase evolved by cycling mutagenesis. Nat Biotechnol 16:657–662
19. **Hoess RH, Abremski K** 1990 The Cre-*lox* recombination system. In: Eckstein F, Lilley DMJ, eds. Nucleic acids and molecular biology. Berlin and Heidelberg: Springer-Verlag
20. **Sauer B, Henderson N** 1988 Site-specific DNA recombination in mammalian cells by the Cre recombinase of bacteriophage P1. Proc Natl Acad Sci USA 85:5166–5170
21. **Albert H, Dale EC, Lee E, Ow DW** 1995 Site-specific integration of DNA into wild-type and mutant lox sites placed in the plant genome. Plant J 7:649–659
22. **Oberdoerffer P, Otipoby KL, Maruyama M, Rajewsky K** 2003 Unidirectional Cre-mediated genetic inversion in mice using the mutant loxP pair lox66/lox71. Nucleic Acids Res 31:e140
23. **Zhang Z, Lutz B** 2002 Cre recombinase-mediated inversion using lox66 and lox71: method to introduce conditional point mutations into the CREB-binding protein. Nucleic Acids Res 30:e90
24. **Crawford LA, Guney MA, Oh YA, Deyoung RA, Valenzuela DM, Murphy AJ, Yancopoulos GD, Lyons KM, Brigstock DR, Economides A, Gannon M** 2009 Connective tissue growth factor (CTGF) inactivation leads to defects in islet cell lineage allocation and β-cell proliferation during embryogenesis. Mol Endocrinol 23:324–336
25. **Logan M, Martin JF, Nagy A, Lobe C, Olson EN, Tabin CJ** 2002

Expression of Cre Recombinase in the developing mouse limb bud driven by a Prxl enhancer. Genesis 33:77–80
26. **Zhang M, Xuan S, Bouxsein ML, von Stechow D, Akeno N, Faugere MC, Malluche H, Zhao G, Rosen CJ, Efstratiadis A, Clemens TL** 2002 Osteoblast-specific knockout of the insulin-like growth factor (IGF) receptor gene reveals an essential role of IGF signaling in bone matrix mineralization. J Biol Chem 277:44005–44012
27. **Nazarenko I, Lowe B, Darfler M, Ikonomi P, Schuster D, Rashtchian A** 2002 Multiplex quantitative PCR using self-quenched primers labeled with a single fluorophore. Nucleic Acids Res 30:e37
28. **Nazarenko I, Pires R, Lowe B, Obaidy M, Rashtchian A** 2002 Effect of primary and secondary structure of oligodeoxyribonucleotides on the fluorescent properties of conjugated dyes. Nucleic Acids Res 30:2089–2195
29. **Nagy TR, Prince CW, Li J** 2001 Validation of peripheral dual-energy x-ray absorptiometry for the measurement of bone mineral in intact and excised long bones of rats. J Bone Miner Res 16:1682–1687
30. **Gazzerro E, Pereira RC, Jorgetti V, Olson S, Economides AN, Canalis E** 2005 Skeletal overexpression of gremlin impairs bone formation and causes osteopenia. Endocrinology 146:655–665
31. **Parfitt AM, Drezner MK, Glorieux FH, Kanis JA, Malluche H, Meunier PJ, Ott SM, Recker RR** 1987 Bone histomorphometry: standardization of nomenclature, symbols, and units. Report of the ASBMR Histomorphometry Nomenclature Committee. J Bone Miner Res 2:595–610
32. **Glatt V, Canalis E, Stadmeyer L, Bouxsein ML** 2007 Age-related changes in trabecular architecture differ in female and male C57BL/6J mice. J Bone Miner Res 22:1197–1207
33. **McCarthy TL, Centrella M, Canalis E** 1988 Further biochemical and molecular characterization of primary rat parietal bone cell cultures. J Bone Miner Res 3:401–408
34. **Zanotti S, Smerdel-Ramoya A, Stadmeyer L, Durant D, Radtke F, Canalis E** 2008 Notch inhibits osteoblast differentiation and causes osteopenia. Endocrinology 149:3890–3899
35. **Kouadjo KE, Nishida Y, Cadrin-Girard JF, Yoshioka M, St-Amand J** 2007 Housekeeping and tissue-specific genes in mouse tissues. BMC Genomics 8:127
36. **Ryseck RP, Macdonald-Bravo H, Mattéi MG, Bravo R** 1991 Structure, mapping, and expression of fisp-12, a growth factor-inducible gene encoding a secreted cysteine-rich protein. Cell Growth Differ 2:225–233
37. **Nakanishi T, Yamaai T, Asano M, Nawachi K, Suzuki M, Sugimoto T, Takigawa M** 2001 Overexpression of connective tissue growth factor/hypertrophic chondrocyte-specific gene product 24 decreases bone density in adult mice and induces dwarfism. Biochem Biophys Res Commun 281:678–681
38. **Rydziel S, Stadmeyer L, Zanotti S, Durant D, Smerdel-Ramoya A, Canalis E** 2007 Nephroblastoma overexpressed (Nov) inhibits osteoblastogenesis and causes osteopenia. J Biol Chem 282:19762–19772
39. **Canalis E, Smerdel-Ramoya A, Durant D, Economides AN, Beamer WG, Zanotti S** 2010 Nephroblastoma overexpressed (NOV) inactivation sensitizes osteoblasts to bone morphogenetic protein-2 but NOV is dispensable for skeletal homeostasis. Endocrinology 151: 221–233
40. **Kutz WE, Gong Y, Warman ML** 2005 WISP3, the gene responsible for the human skeletal disease progressive pseudorheumatoid dysplasia, is not essential for skeletal function in mice. Mol Cell Biol 25:414–421
41. **Nakamura Y, Cui Y, Fernando C, Kutz WE, Warman ML** 2009 Normal growth and development in mice over-expressing the CCN family member WISP3. J Cell Commun Signal 3:105–113
42. **Mandal CC, Ghosh Choudhury G, Ghosh-Choudhury N** 2009 Phosphatidylinositol 3 kinase/Akt signal relay cooperates with smad in bone morphogenetic protein-2-induced colony stimulating factor-1 (CSF-1) expression and osteoclast differentiation. Endocrinology 150:4989–4998
43. **Mochizuki H, Hakeda Y, Wakatsuki N, Usui N, Akashi S, Sato T, Tanaka K, Kumegawa M** 1992 Insulin-like growth factor-I supports formation and activation of osteoclasts. Endocrinology 131:1075–1080
44. **Okamoto M, Murai J, Yoshikawa H, Tsumaki N** 2006 Bone morphogenetic proteins in bone stimulate osteoclasts and osteoblasts during bone development. J Bone Miner Res 21:1022–1033
45. **Sotillo Rodriguez JE, Mansky KC, Jensen ED, Carlson AE, Schwarz T, Pham L, MacKenzie B, Prasad H, Rohrer MD, Petryk A, Gopalakrishnan R** 2009 Enhanced osteoclastogenesis causes osteopenia in twisted gastrulation-deficient mice through increased BMP signaling. J Bone Miner Res 24:1917–1926
46. **Zanotti S, Canalis E** 2010 Notch and the skeleton. Mol Cell Biol 30:886–896